Composite Structures 176 (2017) 294–303

Contents lists available at ScienceDirect

Composite Structures

journal homepage: www.elsevier.com/locate/compstruct

Multiple low-frequency broad band gaps generated by a phononic crystal of periodic circular cavity sandwich plates

Shan Jiang [a,b,c], Hao Chen [a,b], Longxiang Dai [a,b], Hongping Hu [a,b,c,*], Vincent Laude [c]

[a] Department of Mechanics, Huazhong University of Science and Technology, Wuhan 430074, PR China
[b] Hubei Key Laboratory for Engineering Structural Analysis and Safety Assessment, Huazhong University of Science and Technology, Wuhan 430074, PR China
[c] Franche-Comté Electronique Mécanique Thermique et Optique, CNRS UMR 6174, Université de Bourgogne Franche-Comté, Besançon 25030, France

ARTICLE INFO

Article history:
Received 14 November 2016
Revised 20 April 2017
Accepted 22 May 2017
Available online 24 May 2017

ABSTRACT

We propose a new type of phononic crystal (PnC) composed of a periodic alternation of circular cavity sandwich plates. In the low-frequency regime, the crystal can modulate the propagation of flexural waves. Governing equations are deduced basing on the classical theory of coupled extensional and flexural vibrations of plates. The dispersion relation of the infinite PnC is calculated by combining the transfer matrix method with Bloch theory. The dynamic response of the PnC with finite unit cells is further studied with finite element analysis. An experiment is carried out to demonstrate the performance of the PnC in vibration isolation. Numerical results and experimental results both illustrate that the proposed PnC can generate several wide low-frequency Bragg band gaps providing strong attenuation. The dependence of band gaps upon geometric and material parameters is also analyzed in detail in view of vibration isolation applications.

1. Introduction

The propagation of elastic waves in periodic structures has been researched for many years. As artificial periodic structures, phononic crystals (PnCs) can modulate efficiently the propagation of acoustic or elastic waves by a periodic distribution of material properties. One of the most attractive properties of the PnCs is the existence of frequency band gaps, within which acoustic or elastic waves cannot propagate freely without attenuation. In recent years, the PnCs have gained increasing interest, both because of their amazing physical properties and because of their potential applications [1–3]. Moreover, small vibrations on the order of nanometers pose challenges for improving the precision of ultra-precision machine tools and of metrology equipment [4]. Therefore band gap engineering is expected to be an effective measure for vibration isolation.

In order to effectively employ band gaps to isolate vibrations, some challenges have to be faced.

A first challenge is to obtain band gaps with low center frequency. The reason is that the spectra of environmental noise and mechanical vibrations are stronger in the low-frequency range. As they appear as low-frequency branches in dispersion relations [5], flexural waves of elastic thin plates are most commonly used in the PnCs to achieve low-frequency band gaps [6–10]. Furthermore, compared with a rectangular plate, a circular plate has more symmetry and better dynamic characteristics, especially regarding rotary motion. But only few works considered periodic circular plate structures [11–13]. Band gaps can generally be induced by two different mechanisms, which are named Bragg band gaps and locally resonant band gaps [14], respectively. The PnCs showing locally resonant band gaps are also called metamaterials since they possess an effective negative mass in the band gap range [15]. For an elastic wave, a lower frequency means a larger wavelength. Hence, in order to obtain a low-frequency Bragg band gap, a long propagation distance is required. The center frequency of locally resonant band gaps, in contrast, can be reduced since the unit cell incorporates a heavy mass and a soft material, which is equivalent to a mass-spring oscillator with a low resonant frequency. Furthermore, a low-frequency local resonance can be created in piezoelectrics by incorporating a strong inductor [16–18].

A second challenge is to broaden the band gap and a number of efforts have been made in that direction. A hybrid PnC consisting of a bi-prism and an inverted bi-prism was proposed for noise control in a broad bandwidth [19]. A locally resonant beam with multiple arrays of damped resonators can achieve much broader band gaps than a locally resonant beam with only a single array of resonators [20]. A scheme of realizing broadband asymmetric acoustic transmission was proposed by using gradient-index structure. The

* Corresponding author at: Department of Mechanics, Huazhong University of Science and Technology, Wuhan 430074, PR China.
E-mail address: huhp@hust.edu.cn (H. Hu).

http://dx.doi.org/10.1016/j.compstruct.2017.05.048
0263-8223/

asymmetric transmission was found to be valid within a remarkably broad frequency range [21]. The erection of pillars on the solid regions of a plate patterned by a periodic array of holes increased subwavelength band gaps in size by up to a factor of 4 [22]. A one-dimensional finite-sized PnC was proposed to realize broad band-pass, high-performance filtering whose unit cell is configured with two elements having mirrored impedance distributions [23]. A quasi one-dimensional split ring resonator medium was investigated to match the local resonance frequency to the Bragg frequency, thus opening a single band gap which is at the same time very wide and strongly attenuating [24]. A dual-scale PnC slab was used to support two effective spins for phonons over a broad bandwidth [25]. Stacked-structure formed by orthogonally stacking square coated-steel rods embedded in a layer was employed to widen the band gap [26]. Lee et al. [27] investigated the feasibility of broadband sound blocking by introducing rotationally symmetric extensible inclusions.

A third challenge is to achieve strong attenuation. Generally, attenuation can be enhanced by increasing the damping coefficient. Oh et al. [28] showed that air- and metal-embedded viscoelastic PnCs can indeed dissipate more wave energy than pure viscoelastic media in low and high frequency ranges. Frazier et al. [29] studied a dynamic effective mass for the damped metamaterial model to exhibit negative values over a frequency region near the band gap, as in the undamped case. However, for relatively high levels of damping, no frequencies are found in which the effective mass is only negative. In addition, damping can be introduced into piezoelectric PnCs by tuning the resistance of the resonant shunting circuit. For locally resonant band gaps, there exist optimum resistances to obtain a small transmission at the center frequency, while transmission on both sides of the band gap cannot be large [11,12]. Furthermore, transmission decreases when increasing the periodicity number [16,30], with the drawback of making the structure more bulky.

Accordingly, widening locally resonant band gaps but retaining their low center frequency and reducing the center frequency of Bragg band gaps while maintaining their characteristics of broad range are two main research orientations to make the PnC a vibration isolator with good performance. Moreover, a good vibration isolator also requires that the PnC owns some other properties, such as miniature size and load-carrying capacity. Therefore, an appropriate design of a finite PnC structure is critical to have it overcome all these challenges at the same time.

Sandwich structures are widely used in a variety of engineering applications due to their outstanding features, such as a high stiffness-to-mass ratio and easiness of design and manufacture. The high stiffness-to-mass ratio can result in flexural wave propagation at relatively low frequencies and can impart good performance of vibration isolation and sound insulation [31,32]. Band gaps have already been introduced into the analysis and design of sandwich structures to control wave propagation within them [33–36]. Nevertheless, to make the PnC meet the demand of vibration isolators, the band gaps should be further broaden and the operation frequency should be further reduced.

In view of vibration isolation applications, we propose a new PnC of periodic circular cavity sandwich plates. The investigation is focused on wide band gaps with strong attenuation in the low-frequency range. Classical plate theory is first applied to describe the behavior of laminated plates supporting coupled extensional and flexural vibrations. Basing on the equations of motion, the complex band structure and the frequency response function are calculated by the transfer matrix method. In order to evaluate the performance of this PnC for isolating vibration from ultra-precision machines, vibration transmission through a finite structure is further examined using finite element analysis. These numerical simulations confirm the existence of the band gaps predicted by the transfer matrix method. Finally, a first experimental demonstration is reported.

The paper is organized as follows. The mathematical modeling and the equations of motion are investigated in Section 2. A harmonic analysis of the structure is conducted and its solution is obtained in Section 3. Numerical results and comparison with finite element analysis are presented in Section 4. The experiment is performed to demonstrate the effectiveness of the PnC on vibration isolation in Section 5. Finally, some conclusions are drawn in Section 6.

2. The PnC model of periodic circular cavity sandwich plates

The proposed PnC is arrayed periodically by connecting circular cavity sandwich plates in series. A quarter cutaway and a cross sectional views are illustrated in Fig. 1(a) and (b). Each unit cell is a circular cavity sandwich plate. It is composed of a sandwich plate, one ring, and one centered cylinder. The structure is considered a sandwich plate since the only difference with a conventional sandwich plate is the replacement of the interlayer medium by a cavity. The ring and the centered cylinder locate at the outer edge and at the center of the sandwich plate, respectively. The two plates with thickness $2h$ are denoted by I and II, respectively. The PnC structure can be regarded as a folded beam rotated by a complete revolution around one of its sides. Fig. 1(c) illustrates the folded beam in an axisymmetric meridian plane with certain nth unit cell circled by red dashed lines. The outer radius of the ring and the outer and

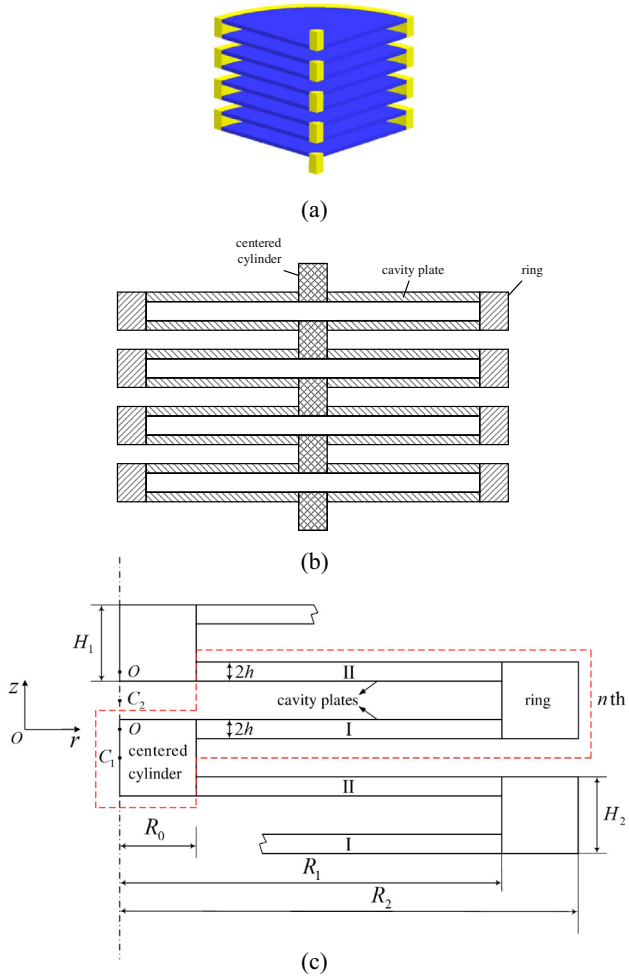

Fig. 1. Quarter cutaway view (a), cross sectional view (b), and axisymmetric sectional view (c) of the PnC of periodic circular cavity sandwich plates.

inner radius of the sandwich plate are represented by R_2, R_1, and R_0. Thicknesses of the centered cylinder and of the ring are denoted by H_1 and H_2, as shown in Fig. 1(c).

The axisymmetric structure can maintain an axisymmetric motion when pulled or pushed along the axial direction. In cylindrical coordinates (r, θ, and z) we consider axisymmetric coupling vibration of the plate between the flexural motion in the z direction and the extensional motion in the r direction. According to the classical theory for plates in coupled extensional and flexural vibrations [37], the nontrivial components of strain can be expressed as

$$S_{rr} = u_{r,r} - zu_{z,rr}, \quad S_{\theta\theta} = \frac{1}{r}(u_r - zu_{z,r}), \tag{1}$$

where $u_r(r,t)$ and $u_z(r,t)$ are the extensional and the flexural displacements of neutral layer of the plate, respectively. They are independent of θ, and the tangential displacement u_θ of neutral layer of the plate can be ignored due to the axisymmetric motion. The convention that a comma followed by an index denotes partial differentiation with respect to the coordinate associated with their index is used.

The constitutive equations, or Hooke's law, for an isotropic material are

$$\begin{aligned} T_{rr} &= (\lambda + 2G)S_{rr} + \lambda S_{\theta\theta} + \lambda S_{zz}, \\ T_{\theta\theta} &= \lambda S_{rr} + (\lambda + 2G)S_{\theta\theta} + \lambda S_{zz}, \\ T_{zz} &= \lambda S_{rr} + \lambda S_{\theta\theta} + (\lambda + 2G)S_{zz}, \end{aligned} \tag{2}$$

where Lame's constants $\lambda = Ev/(1+v)(1-2v)$, $G = E/2(1+v)$. E and v are the Young's modulus and the Poisson's ratio of the elastic material, respectively. For the thin plate, we make the usual stress relaxation condition that $T_{zz} = 0$, so that Eq. (2) can be reduced to

$$\begin{aligned} T_{rr} &= \tfrac{E}{1-v^2}(S_{rr} + vS_{\theta\theta}), \\ T_{\theta\theta} &= \tfrac{E}{1-v^2}(S_{\theta\theta} + vS_{rr}). \end{aligned} \tag{3}$$

The bending moments and shearing force per unit length can be obtained from Eqs. (1) and (3)

$$\begin{aligned} M_r &= \int_{-h}^{h} T_{rr} z\mathrm{d}z = -D_1\left(u_{z,rr} + \tfrac{v}{r}u_{z,r}\right), \\ M_\theta &= \int_{-h}^{h} T_{\theta\theta} z\mathrm{d}z = -D_1\left(vu_{z,rr} + \tfrac{1}{r}u_{z,r}\right), \\ Q_r &= \int_{-h}^{h} T_{rz}\mathrm{d}z = M_{r,r} + \tfrac{M_r - M_\theta}{r} = -D_1\left(\nabla^2 u\right)_{,r}, \end{aligned} \tag{4}$$

where the bending stiffness is $D_1 = 2Eh^3/3(1-v^2)$ and the Laplacian operator is defined as $\nabla^2 = \partial^2/\partial r^2 + \partial/(r\partial r)$. Similarly, the extensional resultants per unit length are

$$\begin{aligned} N_r &= \int_{-h}^{h} T_{rr}\mathrm{d}z = D_2\left(v\tfrac{u_r}{r} + u_{r,r}\right), \\ N_\theta &= \int_{-h}^{h} T_{\theta\theta}\mathrm{d}z = D_2\left(\tfrac{u_r}{r} + vu_{r,r}\right), \end{aligned} \tag{5}$$

where the tensile stiffness is $D_2 = 2Eh/(1-v^2)$.

The plate equations of motion for extension and flexure take the following form

$$N_{r,r} + \frac{N_r - N_\theta}{r} = m\ddot{u}_r, \quad Q_{r,r} + \frac{Q_r}{r} = m\ddot{u}_z, \tag{6}$$

where $m = 2\rho h$ is the mass per unit area of the plates with the density ρ of the isotropic material. A superimposed dot represents derivative with respect to time. Substitution of Eqs. (4) and (5) into Eq. (6) yields

$$\begin{aligned} -D_1\nabla^2\nabla^2 u_z &= m\ddot{u}_z, \\ D_2\left(u_{r,rr} + \tfrac{1}{r}u_{r,r} - \tfrac{u_r}{r^2}\right) &= m\ddot{u}_r, \end{aligned} \tag{7}$$

The centered cylinders and rings are assumed to be rigid bodies, i.e. their deformation is ignored. The forces and displacements of centered cylinders and rings are presented in Fig. 2. At the interface between the sandwich plate and the centered cylinder or the ring, extensional displacement, flexural displacement, rotation angle, extensional force, shear force, and bending moment meet continuity conditions.

Considering axisymmetric vibration of the sandwich plate, continuity conditions at the interfaces between the centered cylinder of the nth unit cell and the plate II of the (n-1)th unit cell, and between the centered cylinder and the plate I of the nth unit cell, are

$$\begin{aligned} &u_r^{(n-1)\mathrm{II}}(R_0,t) = u_r^{(n)\mathrm{I}}(R_0,t), \\ &u_z^{(n-1)\mathrm{II}}(R_0,t) = u_z^{(n)\mathrm{I}}(R_0,t), \\ &u_{z,r}^{(n-1)\mathrm{II}}(R_0,t) = u_{z,r}^{(n)\mathrm{I}}(R_0,t) = 0, \\ &-2\pi R_1\left[N_r^{(n-1)\mathrm{II}}(R_0,t) + N_r^{(n)\mathrm{I}}(R_0,t)\right] = 0, \\ &2\pi R_0\left[Q_r^{(n-1)\mathrm{II}}(R_0,t) + Q_r^{(n)\mathrm{I}}(R_0,t)\right] = m_1\ddot{u}_z^{(n)C_1}(t), \\ &2\pi R_1\Big\{-M_r^{(n-1)\mathrm{II}}(R_0,t) - M_r^{(n)\mathrm{I}}(R_0,t) + R_0\left[Q_r^{(n-1)\mathrm{II}}(R_0,t) + Q_r^{(n)\mathrm{I}}(R_0,t)\right] \\ &\quad + \left(\tfrac{H_1}{2} - h\right)\left[N_r^{(n-1)\mathrm{II}}(R_0,t) - N_r^{(n)\mathrm{I}}(R_0,t)\right]\Big\} = 0, \end{aligned} \tag{8}$$

where superscripts (n), I and II, C_1 represent the nth unit cell, plate I and plate II, and the centered cylinder, respectively. $m_1 = \rho_1\pi R_0^2 H_1$ is the mass of the centered cylinder with material density ρ_1. By ignoring the deformation of the centered cylinder, the relationship between the displacement of the two plates and of the centroid of centered cylinders is

$$u_z^{(n)C_1}(t) = u_z^{(n)\mathrm{I}}(R_0,t). \tag{9}$$

Similarly, the continuity conditions at the connection point of two plates in an arbitrary unit cell is governed by

$$\begin{aligned} &u_r^{(n)\mathrm{I}}(R_1,t) = u_r^{(n)\mathrm{II}}(R_1,t), \\ &u_z^{(n)\mathrm{I}}(R_1,t) = u_z^{(n)\mathrm{II}}(R_1,t), \\ &u_{z,r}^{(n)\mathrm{I}}(R_1,t) = u_{z,r}^{(n)\mathrm{II}}(R_1,t), \\ &-2\pi R_1\left[N_r^{(n)\mathrm{I}}(R_1,t) + N_r^{(n)\mathrm{II}}(R_1,t)\right] = 0, \\ &-2\pi R_1\left[Q_r^{(n)\mathrm{I}}(R_1,t) + Q_r^{(n)\mathrm{II}}(R_1,t)\right] = m_2\ddot{u}_z^{(n)C_2}(t), \\ &2\pi R_1\Big\{M_r^{(n)\mathrm{I}}(R_1,t) + M_r^{(n)\mathrm{II}}(R_1,t) - R_1\left[Q_r^{(n)\mathrm{I}}(R_1,t) + Q_r^{(n)\mathrm{II}}(R_1,t)\right] \\ &\quad + \left(\tfrac{H_2}{2} - h\right)\left[N_r^{(n)\mathrm{II}}(R_1,t) - N_r^{(n)\mathrm{I}}(R_1,t)\right]\Big\} = 0, \end{aligned} \tag{10}$$

where superscript C_2 represents the parameters of the ring. $m_2 = \rho_2\pi(R_2^2 - R_1^2)H_2$ is the mass of the ring with material density ρ_2. The relationship between the displacements of the centroids of the rings and of the plates is

$$u_z^{(n)C_2}(t) = u_z^{(n)\mathrm{II}}(R_1,t). \tag{11}$$

The frequency response function (FRF) is defined by $20\log10(|u_{\mathrm{out}}/u_{\mathrm{in}}|)$, where u_{out} and u_{in} are displacement amplitudes of centered cylinders on the top and bottom, which is often used to represent wave propagation through a finite periodic structure. For the PnCs with the finite unit cells, the boundary conditions can be written as

$$\begin{aligned} &u_r^{(1)\mathrm{I}}(R_0,t) = 0, \quad u_z^{(1)\mathrm{I}}(R_0,t) = u_{in}e^{\mathrm{i}\omega t}, \quad u_{z,r}^{(1)\mathrm{I}}(R_0,t) = 0, \\ &u_r^{(N)\mathrm{II}}(R_0,t) = 0, \quad 2\pi R_0 Q_r^{(N)\mathrm{II}}(R_0,t) = m_1\ddot{u}_z^{(N)\mathrm{II}}(R_0,t), \\ &-M_r^{(N)\mathrm{II}}(R_0,t) + R_0 Q_r^{(N)\mathrm{II}}(R_0,t) + \left(\tfrac{H_1}{2} - h\right)N_r^{(N)\mathrm{II}}(R_0,t) = 0, \end{aligned} \tag{12}$$

where i and ω are the imaginary unit and the angular frequency. $u_z^{(N)\mathrm{II}}$ is equal to the displacement of the centered cylinder of the

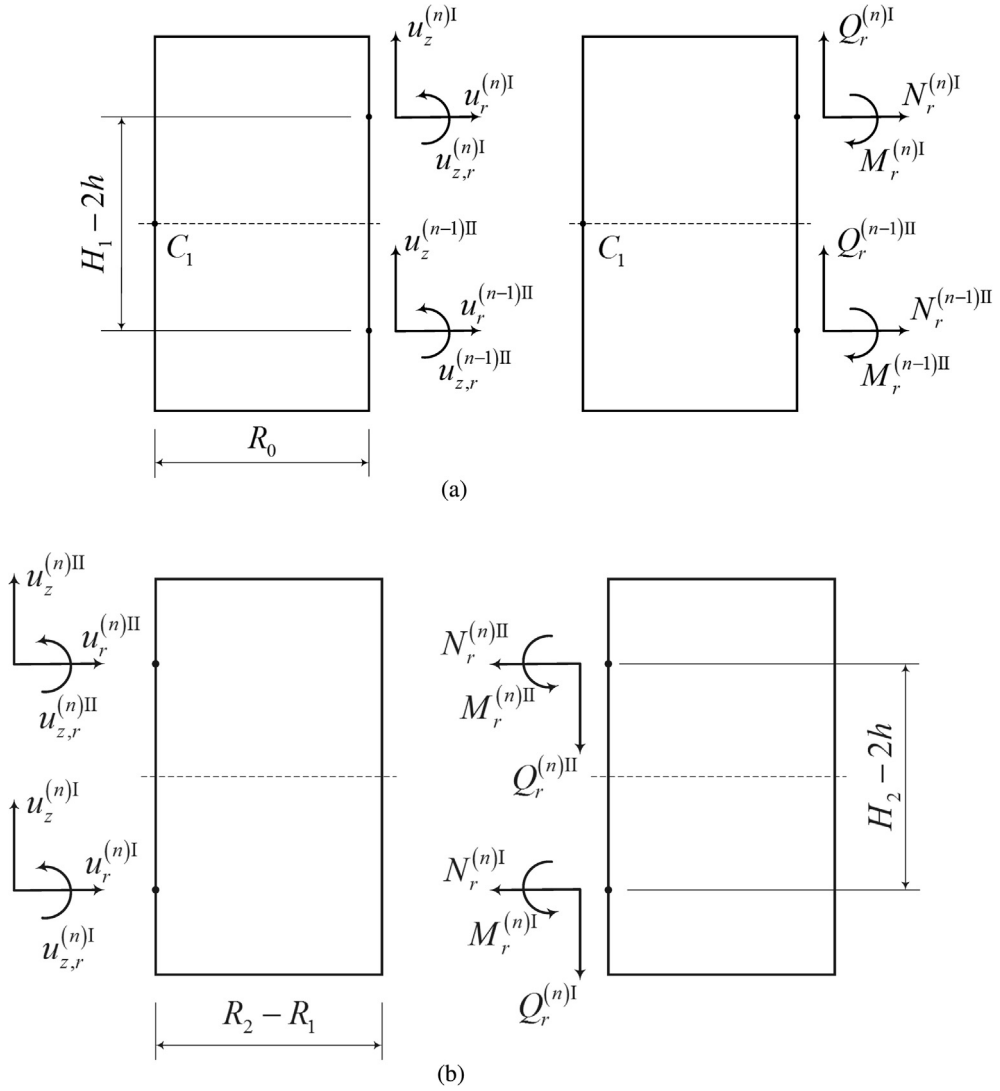

Fig. 2. Sketch of the displacements and forces acting on (a) centered cylinders and (b) rings.

top. Therefore its amplitude is considered as the output displacement u_{out}.

3. Complex band structure of periodic circular cavity sandwich plates

For harmonic motions, we use the complex notation

$$\{u_r(r,t), u_z(r,t)\} = \mathrm{Re}\{[U_r(r), U_z(r)]e^{\mathrm{i}\omega t}\}, \tag{13}$$

The equations of motion (7) become

$$\begin{aligned} &D_1\nabla^2\nabla^2 U_z = m\omega^2 U_z, \\ &D_2\left(U_{r,rr} + \tfrac{1}{r}U_{r,r} - \tfrac{U_r}{r^2}\right) = -m\omega^2 U_r. \end{aligned} \tag{14}$$

The general solution for Eq. (14) can be written as

$$\begin{aligned} U_z &= A_1 J_0(\lambda_1 r) + A_2 I_0(\lambda_1 r) + A_3 Y_0(\lambda_1 r) + A_4 K_0(\lambda_1 r), \\ U_r &= A_5 J_1(\lambda_2 r) + A_6 Y_1(\lambda_2 r), \end{aligned} \tag{15}$$

where $\lambda_1 = \sqrt[4]{m\omega^2/D_1}$ and $\lambda_2 = \sqrt{m\omega^2/D_2}$, A_i (i = 1, 2, …, 6) are undetermined constants. J_α and Y_α are Bessel functions of the first kind and second kind, I_α and K_α are modified Bessel functions of the first kind and second kind, α (= 0, 1) refers to the corresponding order of Bessel functions.

From Eqs. (4), (5), and (15), the continuity conditions of Eq. (10) can be written in matrix form

$$\mathbf{K}_1\varphi_1^{(n)} = \mathbf{K}_2\varphi_2^{(n)}, \tag{16}$$

where $\mathbf{K_1}$ and $\mathbf{K_2}$ are 6 × 6 square matrices relating coefficients $\varphi_1^{(n)}$ and $\varphi_2^{(n)}$, with $\varphi_j^{(n)} = \left[A_{j1}^{(n)}\ A_{j2}^{(n)}\ A_{j3}^{(n)}\ A_{j4}^{(n)}\ A_{j5}^{(n)}\ A_{j6}^{(n)}\right]^{\mathrm{T}}$, $j = 1, 2$ corresponding to plate I or II in the unit cell. Similarly, the continuity conditions of Eq. (8) can be expressed as

$$\mathbf{H}_2\varphi_2^{(n-1)} = \mathbf{H}_1\varphi_1^{(n)}, \tag{17}$$

where $\mathbf{H_1}$ and $\mathbf{H_2}$ are also 6 × 6 square matrices.

From Eqs. (16) and (17), the linear relationship between undetermined constants of plates II in two neighboring unit cells becomes

$$\varphi_2^{(n)} = \mathbf{T}\varphi_2^{(n-1)}, \tag{18}$$

where $\mathbf{T} = \mathbf{K}_2^{-1}\mathbf{K}_1\mathbf{H}_1^{-1}\mathbf{H}_2$ is the transfer matrix from the (n–1)th to the nth cell. Note that all matrices depend explicitly on the frequency.

According to Bloch theory, we have the periodic condition

$$\varphi_2^{(n)} = e^{\mathrm{i}ka}\varphi_2^{(n-1)}, \tag{19}$$

where k is the Bloch-Floquet wave vector, $a = 2(R_1 - R_0)$ is the lattice constant of the periodic structure. From Eqs. (18) and (19), nontrivial solutions may exist if the determinant satisfies

$$\det\left[\mathbf{T}(\omega) - e^{ika}\mathbf{I}\right] = 0. \tag{20}$$

For a given ω, Eq. (20) is an eigenvalue equation that gives the admissible values of k. The real part of k is the wavenumber, which is used to describe wave propagation phenomena. When k is a real number, a flexural wave can propagate freely. On the contrary, a complex k means the wave is evanescent and thus that its frequency lies in a band gap. An attenuation constant μ is defined by the product of the imaginary part of k with the lattice constant a, in order to measure the decay of the amplitude when the elastic wave propagates from one period to the next.

While for the finite PnC, $12N$ unknows exists if the PnC has N unit cells, which can be solved by 6 equations of boundary conditions (12), $6N$ equations of continuity conditions (10) within the same unit cells, and $6(N\text{-}1)$ equations of continuity conditions (8) between the neighboring unit cells. Hence the frequency response function of the finite PnCs is obtained.

4. Numerical results and discussion

Using metallic material is helpful to improve the load-carrying capacity of the PnC because of the high strength. As a numerical example, Copper is chosen as the material for all parts of the periodic circular cavity sandwich plates. Thus densities $\rho = \rho_1 = \rho_2 = 8900$ kg/m^3, Young's modulus $E = 120$ GPa and Poisson's ratio $v = 0.3$. Geometric parameters of the unit cell are $R_0 = 5$ mm, $R_1 = 65$ mm, $R_2 = 70$ mm, $H_1 = H_2 = 10$ mm, and $h = 1$ mm. These parameters are fixed unless otherwise stated.

The complex band structure of the infinite periodic structure is illustrated in Fig. 3, where the real part of the complex wave vector and the absolute value of the imaginary part of the complex wave vector are illustrated in Fig. 3, respectively. As the transmission matrix is of size 6×6, there are in principle a maximum of 6 eigenvalues. Four of them are found numerically to be always equal to ± 0 or $\pm\pi/a$, corresponding to rigid body motions of the plates that must be discarded. The remaining two eigenvalues are flexural waves propagating either upward or downward. Henceforth the presented complex band structure must be understood for flexural waves only. Three broad and complete band gaps of the Bragg type can be found within the range 0–3500 Hz, whose frequency spans are 364–812 Hz, 1038–2171 Hz, 2625–2975 Hz. It has been observed that unlike local resonances that generate a sharp maximum attenuation at a certain frequency and a highly asymmetric attenuation profile, Bragg scattering produces symmetric frequency-dependent attenuation functions [38,39]. As can be seen from Fig. 3(b), the three gaps are all Bragg band gaps. The gap-to-mid-gap ratio is used to measure the performance of band gaps. A large gap-to-mid-gap ratio means both low-frequency operation and wide band gap. The gap-to-mid-gap ratios corresponding to three band gaps are 76%, 71% and 13%, respectively. The first two ratios are larger than most of those listed in Table 1 of Ref. [40]. Moreover, although a Bragg band gap, the first band gap of our structure has a lower frequency of 364 Hz. This value compares favorably with the locally resonant band gap generated by a 70 mm-long rods woodpile PnC [41], for instance.

The vibration and bending modes at the edges of the first Brillouin zone (external points defining the band gaps) are now presented in Fig. 4. They are calculated using the finite element method (FEM). Without loss of generality and intrinsic essence, we choose a unit cell with longitudinal symmetry in order to show results that are more intuitive than the theoretical analysis. We observe that the two cavity plates in the unit cell move in phase for lower points, such as S1, S3, S5, of all band gaps, whereas they move out of phase for upper points, such as S2, S4, S6, of all band gaps.

The proposed PnC thus owns some qualities to obtain multiple low-frequency broad band gaps. First, the periodic cavity sandwich plate structure can transform low-frequency vibrations into low-frequency flexural waves. Second, owing to the periodic structure of cavity sandwich plates, the PnC extends the flexural wave propagation path but the structure size remains small. Third, as can be seen from Fig. 4, the flexural wave propagates along the cavity plates, while the centered cylinder and the ring only vibrate up and down with little deformation. Thus, it is quite reasonable to

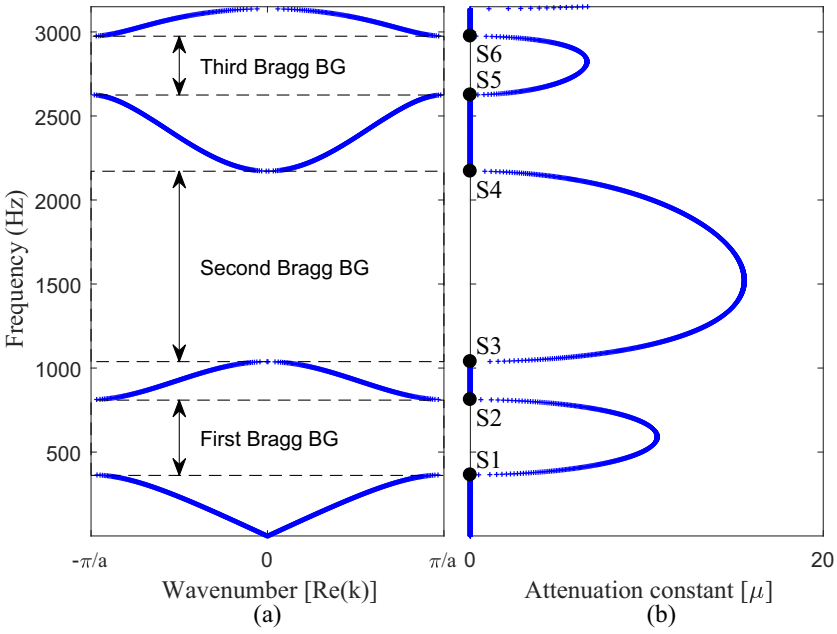

Fig. 3. Complex band structure of the PnC of periodic circular cavity sandwich plates. (a) Wave number Re(k) and (b) attenuation constant $\mu = \mathrm{Im}(k)a$ as a function of frequency. The PnC is made of copper.

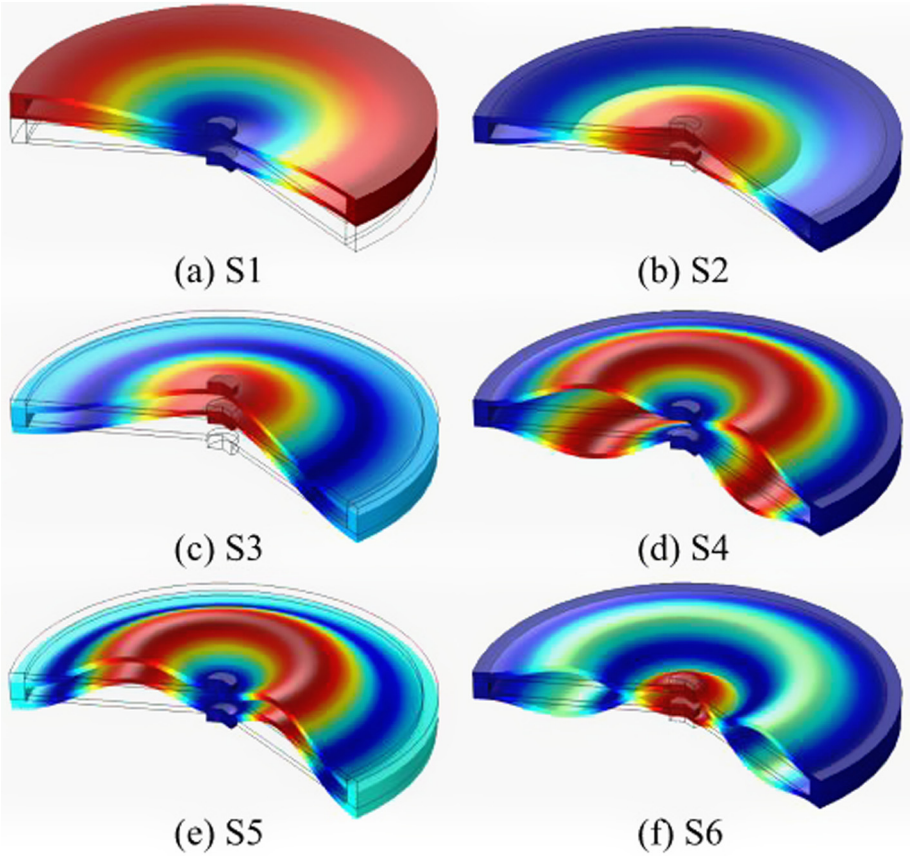

Fig. 4. Vibration modes (a)-(e) correspond to external points S1-S6 of band gaps in Fig. 3(b), respectively.

assume that the centered cylinder and the ring are rigid bodies in the theoretical analysis. Compared with the plate, the centered cylinder and the ring have an infinite bending stiffness. The bending stiffness varies periodically and enormously among the centered cylinders, the plates and the rings. The flexural wave is alternately modulated by the centered cylinders, the plates and the rings of the periodic structure. Strong reflected waves are generated when the flexural wave meets the centered cylinders and the rings. The transmitted waves are thus easily offset by the strong reflected waves. Consequently, multiple broad band gaps are opened due to the mismatch in the bending stiffness. Finally, compared with periodic folding beam-type PnCs [42], the proposed

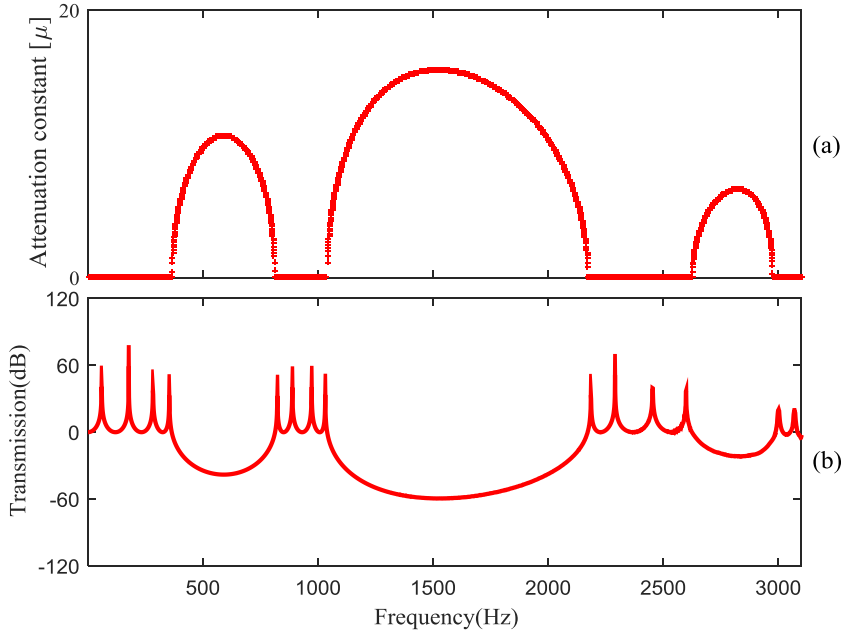

Fig. 5. (a) Attenuation constants μ of the infinite system and (b) frequency response factor of the finite periodic structure with four unit cells. The PnC is made of copper.

PnC can counteract the motion of extension of the plate due to its axisymmetric structure.

For PnCs, certain frequency ranges of the finite periodic structure with a good vibration reduction performance correspond to the band gaps of the infinite periodic system, if the same unit cell is adopted. The characteristic of the finite periodic structure is thus often employed to verify the band structure of the infinite periodic system. Fig. 5 illustrates the attenuation constants of the infinite system in (a) and the transmission factor of the periodic structure with four unit cells in (b) versus frequency. In order to study vibration isolation in the low-frequency range, we focus on frequencies below 3500 Hz. As shown in Fig. 5(b), the wave is seen to be attenuated in some frequency range if the transmission factor is less than zero. The band gap is induced by the interaction between the incident wave, the reflected wave and the transmitted wave within an infinite periodic system. Similarly, as the elastic wave is modulated by the finite periodic structure, attenuation can appear but also resonances or anti-resonances that were not present in the infinite system. Overall, the finite periodic structure shows a good performance for vibration reduction in the frequency ranges corresponding to the band gaps of the infinite system. It is also found that the transmission properties of the finite periodic structure agree well with the dispersion relation of the infinite system. Nonetheless, some transmission peaks arise in pass bands corresponding to the resonant frequencies of the finite periodic structure, which imply the amplification of vibration at the corresponding frequencies. The peaks in the high frequency region could be further cut down by the introduction of damping and those in the low-frequency region could be reduced by active control. Accordingly, it is meaningful to cover a wide frequency range of vibration since the proposed periodic structure owns several broad band gaps.

In order to validate the theoretical model, the frequency response function of the finite periodic structure was further calculated by FEM implemented with the ANSYS software. Three-dimensional element SOLID45 is chosen for this model. A three-dimensional FEM model is meshed by hexahedral-shaped volume elements, as shown in Fig. 6. Note that the FEM does not make any assumption regarding flexural wave propagation but instead considers general elastic wave propagation in three-dimensional solids. The comparison of frequency response function curves between model and numerical simulation is plotted in Fig. 7. The agreement is found to be fairly good, especially in the low-frequency range. Indeed, a peak "A" in the transmission inside the band gap can be noticed around 1.9 kHz. We have added an inset to illustrate the deformation and the distribution of displacements when a vibrational source at this frequency is imposed on one end of the PnC. A strong attenuation is observed on propagation through four unit cells of the PnC. The particular mode of propagation indeed corresponds to a surface mode as reported in [41,43].

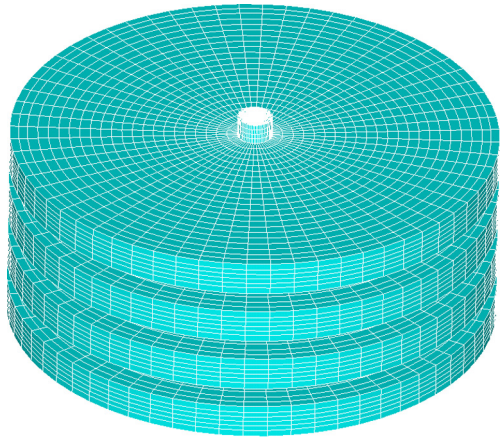

Fig. 6. Three-dimensional mesh of the finite element model of the PnC of periodic circular cavity sandwich plates.

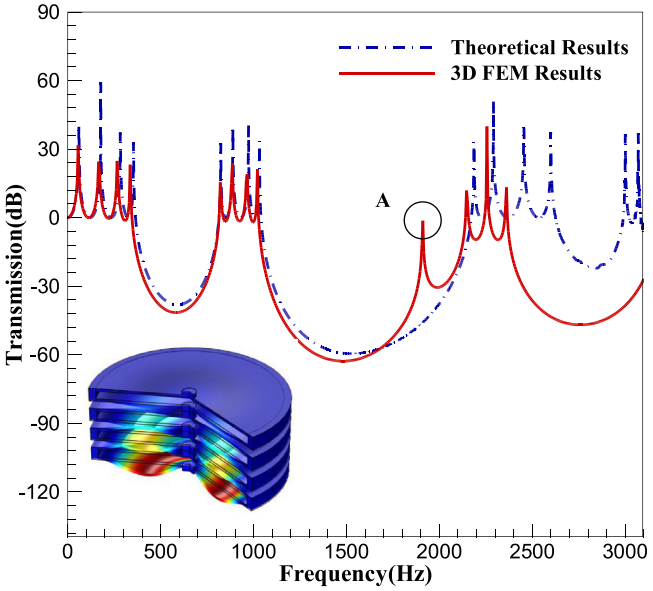

Fig. 7. Comparison on FRF curves of a finite structure with 4 unit cells obtained with either the theoretical model or a 3D finite element model. The inset shows the deformation and the distribution of displacements when a vibrational source at frequency of peak "A" is imposed on one end of the PnC. The PnC is made of copper.

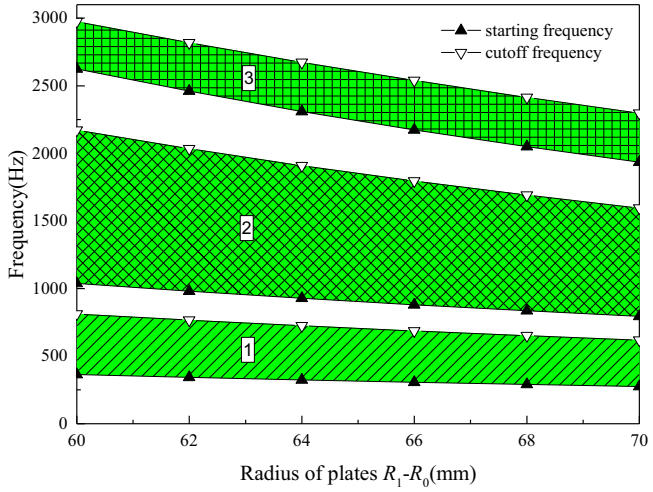

Fig. 8. Effect of the radius R_1-R_0 of the cavity sandwich plates on the first three band gaps. The PnC is made of copper.

Next, we investigate the dependence of band gaps on the geometrical parameters. The radius R_1-R_0 of the cavity sandwich plates can be considered as the lattice constant of the proposed PnC. Fig. 8 presents the evolution of the first three band gaps as a function of the lattice constant R_1-R_0. One can easily observe that the center frequencies of all band gaps decrease and that the band gaps become narrower with the increase of R_1-R_0. It is well known that Bragg scattering depends solely on the wave interferences that take place within the periodic structure. Since the band gaps are derived from Bragg scattering, the lattice constant R_1-R_0 indeed has a significant influence on the band gaps of the proposed PnC.

Finally, the influence of material parameters on the transmission of a finite system with four unit cells is investigated in

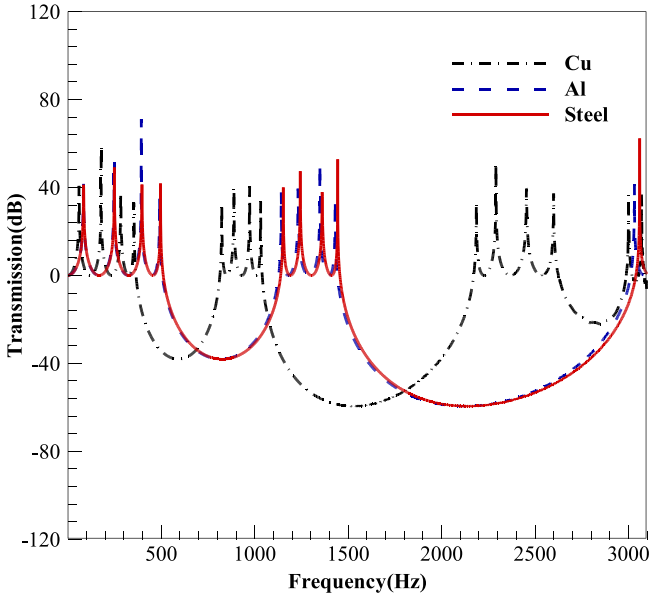

Fig. 9. Effect of material parameters on the transmission of the finite system with four unit cells.

Fig. 9. Three common metallic materials are chosen: Aluminum (Al, $\rho = 2700$ kg/m^3, $E = 70$ GPa, $\nu = 0.3$), mild Steel (Steel, $\rho = 7800$ kg/m^3, $E = 206$ GPa, $\nu = 0.3$), and Copper (Cu, $\rho = 8900$ kg/m^3, $E = 120$ GPa, $\nu = 0.3$). The periodic circular cavity sandwich plates have almost the same transmission properties when material parameters are chosen as Al and Steel. To explain this observation, we can infer from Eq. (15) that the characteristic roots λ_1 and λ_2 of the equations of motion (14) depend on m/D_1 and m/D_2, respectively. Furthermore, m/D_1 and m/D_2 are both proportional to ρ/E. Therefore, the dynamical properties of the finite system are governed by the value of ρ/E for given boundary conditions and structure sizes. For comparison, the ρ/E of Steel, Al and Cu are equal to 37.86, 38.57, and 74.17 s^2/m^2, respectively. It can be seen that the values ρ/E of Al and mild Steel almost match. In addition, the center frequencies of band gaps all decrease when increasing ρ/E. This is consistent with the fact that materials with a large ρ/E like Epoxy (Epoxy, $\rho = 1180$ kg/m^3, $E = 4.35$ GPa, $\nu = 0.37$ with $\rho/E = 271.26$ s^2/m^2) are widely used in PnCs to obtain low-frequency band gaps.

5. Experiment and results

To demonstrate the effectiveness for the structure on vibration isolation, we manufactured a steel PnC (label E in Fig. 10) of circular cavity sandwich plates with four unit cells and the following geometric properties. The thicknesses of the plates, the centered cylinder, and the ring are $2h = 2$ mm, $H_1 = 18$ mm, and $H_2 = 10$ mm, respectively. The radius of the centered cylinder, the outer radius of the plates, and the outer radius of the ring are $R_0 = 6$ mm, $R_1 = 60$ mm, and $R_2 = 65$ mm, respectively. The connections between the plates and the ring are all welded. The cavity plate is joined with the centered cylinder by a screw bolt. The installation of the sample and the experimental apparatus are illustrated in Fig. 10. The white noise signals between 1 Hz and 5000 Hz are generated by a signal generator [Sinocera piezotronics, Inc., YE1311] (label B in Fig. 10). The signals are further amplified by a power amplifier [Sinocera piezotronics, Inc., YE5874A] (label C), and are applied to the vibration exciter [Sinocera piezotronics, Inc., JZK-50] (label D). A couple of accelerometers [X&K Tech., XK101S] (label F and G) with operating frequency scope of 1 to 5000 Hz are used to measure the input and the output accelerators. One accelerometer is installed between the vibration exciter and one end of the PnC. The other accelerometer is mounted on the other end of the PnC. The two accelerometers are linked to the dynamic signal collector [uTekL, uT3404FRS-DI] (label A). The measured input and output accelerators are then analyzed by acquisition and analysis system software [uTekL, uTekSs-V2004] on the computer.

The measured transmission of the PnC is shown in Fig. 11. The frequency in three ranges of 817–1228 Hz, 1434–3406 Hz, and

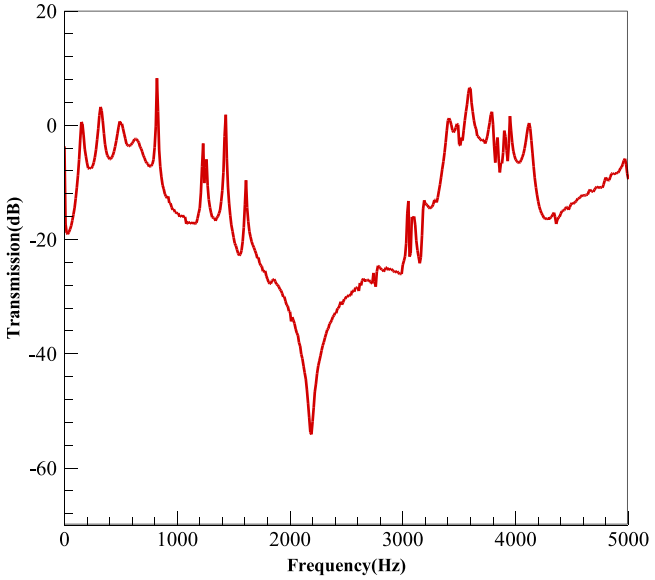

Fig. 11. Measured transmission versus frequency.

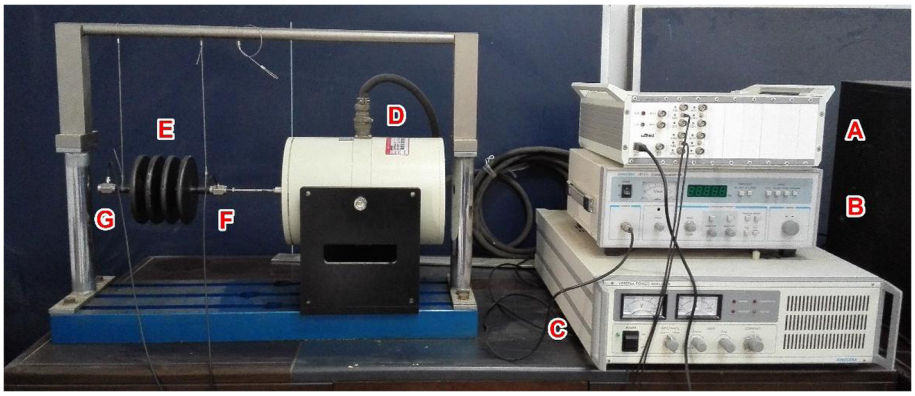

Fig. 10. Installation of the sample and experimental apparatus. The PnC sample is made of steel.

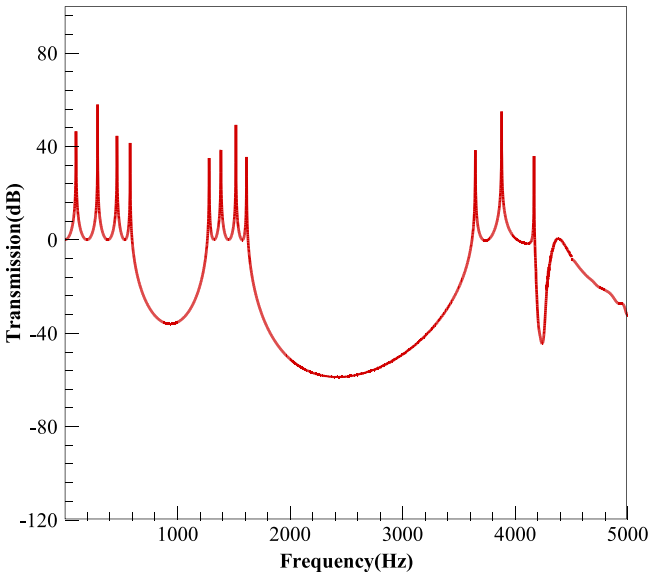

Fig. 12. Calculated transmission versus frequency obtained with the transfer matrix model.

4120–5000 Hz has a larger attenuation than the other frequencies. The maximum of the attenuation reaches to 47.5 dB at 2186 Hz. The three frequency ranges correspond to the first three band gaps. Therefore the low-frequency and broad band gaps with strong attenuation can be achieved by the PnC of circular cavity sandwich plates.

Theoretical result of transmission versus frequency is also illustrated in Fig. 12. All the geometric and material parameters in theoretical calculations are the same as in the experiment. The calculated transmission curve demonstrates that the first three band gaps are 579–1281 Hz, 1613–3647 Hz, and 4168–5000 Hz. The vibration at 2427 Hz has a maximum attenuation of 59 dB. The calculated frequencies of the three band gaps match fairly well with the measured values. In addition, the measured attenuation has an approximate maximum as the calculated attenuation, and the two maximums arise at two close frequencies. The measured transmissions are smaller than the theoretical results at the pass bands, mainly because structural damping has not been taken into account for calculations.

6. Conclusion

A new phononic crystal composed of periodic circular cavity sandwich plates has been proposed to control the propagation of elastic waves. A theoretical solution for coupled extensional and flexural motions of elastic thin plates was obtained. The numerical results illustrate that several low-frequency and broad band gaps with strong attenuation can be induced. Moreover, the proposed PnC has a small size and an excellent load-carrying capacity. We also conducted some comparison between the axisymmetric theoretical model and a three-dimensional finite element method. The theoretical results are found to be in good agreement with numerical simulations. The low-frequency and broad band gaps were also verified by experiment. Thanks to its properties, the proposed PnC of periodic circular cavity sandwich plates could be implemented in engineering applications as a vibration isolator or a noise insulator.

Acknowledgment

This work was supported by the National Natural Science Foundation of China (Nos.11272126, 51435006, and 51421062), the Fundamental Research Funds for the Central Universities, HUST: Nos. 2016JCTD114 and 2015TS121. Hu and Jiang also thank to support of China Scholarship Council (Nos. 201606165026 and 201606160045).

References

[1] Yang S, Page J, Liu Z, Cowan M, Chan C, Sheng P. Focusing of sound in a 3D phononic crystal. Phys Rev Lett 2004;93:024301.
[2] Khelif A, Choujaa A, Benchabane S, Djafari-Rouhani B, Laude V. Guiding and bending of acoustic waves in highly confined phononic crystal waveguides. Appl Phys Lett 2004;84:4400–2.
[3] Hussein MI, Leamy MJ, Ruzzene M. Dynamics of phononic materials and structures: Historical origins, recent progress, and future outlook. Appl Mech Rev 2014;66:040802.
[4] Chen XD, Chen H, Luo X, Ye YX, Hu YT, Xu JQ. Air vortices and nano-vibration of aerostatic bearings. Tribol Lett 2011;42:179–83.
[5] Yang JS. The mechanics of piezoelectric structures. Singapore: World Scientific; 2006.
[6] Spadoni A, Ruzzene M, Cunefare K. Vibration and wave propagation control of plates with periodic arrays of shunted piezoelectric patches. J Intell Mater Syst Struct 2009;20:979–90.
[7] Song Y, Feng L, Wen J, Yu D, Wen X. Analysis and enhancement of flexural wave stop bands in 2D periodic plates. Phys Lett A 2015;379:1449–56.
[8] Claeys CC, Vergote K, Sas P, Desmet W. On the potential of tuned resonators to obtain low-frequency vibrational stop bands in periodic panels. J Sound Vib 2013;332:1418–36.
[9] Brun M, Movchan AB, Jones IS. Phononic band gap systems in structural mechanics: Finite slender elastic structures and infinite periodic waveguides. J Vib Acoust 2013;135:041013.
[10] Xiao Y, Wen JH, Wen XS. Flexural wave band gaps in locally resonant thin plates with periodically attached spring-mass resonators. J Phys D Appl Phys 2012;45:195401–12.
[11] Dai LX, Hu HP, Jiang S, Chen XD. Two kinds equal frequency circuits to achieve locally resonant band gap of a circular plate attached alternately by Piezoelectric Unimorphs. Acta Mech Solida Sin 2016;29:502–13.
[12] Dai LX, Jiang S, Lian ZY, Hu HP, Chen XD. Locally resonant band gaps achieved by equal frequency shunting circuits of piezoelectric rings in a periodic circular plate. J Sound Vib 2015;337:150–60.
[13] Shu H, Zhao L, Shi X, Liu W, Shi D, Kong F. Torsional wave propagation in a circular plate of piezoelectric radial phononic crystals. J Appl Phys 2015;118:2159–64.
[14] Liu ZY, Zhang XX, Mao YW, Zhu YY, Yang ZY, Chan CT, et al. Locally resonant sonic materials. Science 2000;289:1734–6.
[15] Chen YY, Hu J, Huang GL. A design of active elastic metamaterials for control of flexural waves using the transformation method. J Intell Mater Syst Struct 2015.
[16] Wang G, Chen SB, Wen JH. Low-frequency locally resonant band gaps induced by arrays of resonant shunts with Antoniou's circuit: experimental investigation on beams. Smart Mater Struct 2011;20:015026.
[17] Casadei F, Ruzzene M, Dozio L, Cunefare K. Broadband vibration control through periodic arrays of resonant shunts: experimental investigation on plates. Smart Mater Struct 2010;19:015002.
[18] Chen SB, Wang G, Wen JH, Wen XS. Wave propagation and attenuation in plates with periodic arrays of shunted piezo-patches. J Sound Vib 2013;332:1520–32.
[19] Yoo S, Kim YJ, Kim YY. Hybrid phononic crystals for broad-band frequency noise control by sound blocking and localization. J Acoust Soc Am 2012;132:411–6.
[20] Xiao Y, Wen JH, Wen XS. Broadband locally resonant beams containing multiple periodic arrays of attached resonators. Phys Lett A 2012;376:1384–90.
[21] Li RQ, Liang B, Li Y, Kan WW, Zou XY, Cheng JC. Broadband asymmetric acoustic transmission in a gradient-index structure. Appl Phys Lett 2012;101:263502.
[22] Bilal OR, Hussein MI. Trampoline metamaterial: local resonance enhancement by springboards. Appl Phys Lett 2013;103:111901.
[23] Lee IK, Kim YJ, Oh JH, Kim YY. One-dimensional broadband phononic crystal filter with unit cells made of two non-uniform impedance-mirrored elements. AIP Adv 2013;3:226–8.
[24] Kaina N, Fink M, Lerosey G. Composite media mixing Bragg and local resonances for highly attenuating and broad bandgaps. Sci Rep 2013;3:3240.
[25] Mousavi SH, Khanikaev AB, Zheng W. Topologically protected elastic waves in phononic metamaterials. Nat Commun 2015;6:8682.
[26] Chen M, Meng D, Zhang H, Jiang H, Wang Y. Resonance-coupling effect on broad band gap formation in locally resonant sonic metamaterials. Wave Motion 2016;63:111–9.
[27] Lee JS, Yoo S, Ahn YK, Kim YY. Broadband sound blocking in phononic crystals with rotationally symmetric inclusions. J Acoust Soc Am 2015;138.
[28] Hwan OhJ, Jae Kim Y, Young Kim Y. Wave attenuation and dissipation mechanisms in viscoelastic phononic crystals. J Appl Phys 2013;113:106101.
[29] Frazier MJ, Hussein MI. Generalized Bloch's theorem for viscous metamaterials: dispersion and effective properties based on frequencies and wavenumbers that are simultaneously complex. CR Phys 2016;17:565–77.

[30] Wang G, Yu DL, Wen JH, Liu YZ, Wen XS. One-dimensional phononic crystals with locally resonant structures. Phys Lett A 2004;327:512–21.
[31] Thamburaj P, Sun J. Effect of material and geometry on the sound and vibration transmission across a sandwich beam. J Vib Acoust 2001;123:205–12.
[32] Sorokin SV. Vibrations of and sound radiation from sandwich plates in heavy fluid loading conditions. Compos Struct 2000;48:219–30.
[33] Chen J, Sun C. Wave propagation in sandwich structures with resonators and periodic cores. J Sandwich Struct Mater 2013;15:359–74.
[34] Cheng Y, Liu X, Wu D. Band structure of a phononic crystal plate in the form of a staggered-layer structure. J Appl Phys 2011;109:064904.
[35] Song Y, Feng L, Wen J, Yu D, Wen X. Reduction of the sound transmission of a periodic sandwich plate using the stop band concept. Compos Struct 2015;128:428–36.
[36] Liu XF, Wang YF, Wang YS, Zhang CZ. Wave propagation in a sandwich plate with a periodic composite core. J Sandwich Struct Mater 2014;16:319–38.
[37] Reddy JN. Mechanics of laminated composite plates and shells: theory and analysis. London: CRC Press; 2004.
[38] Xiao Y, Wen JH, Yu DL, Wen XS. Flexural wave propagation in beams with periodically attached vibration absorbers: band-gap behavior and band formation mechanisms. J Sound Vib 2013;332:867–93.
[39] Liu L, Hussein MI. Wave motion in periodic flexural beams and characterization of the transition between bragg scattering and local resonance. J Appl Mech 2012;79:011003.
[40] D'Alessandro L, Belloni E, Ardito R, Corigliano A, Braghin F. Modeling and experimental verification of an ultra-wide bandgap in 3D phononic crystal. Appl Phys Lett 2016;109:221907.
[41] Kim E, Yang J. Wave propagation in single column woodpile phononic crystals: formation of tunable band gaps. J Mech Phys Solids 2014;71:33–45.
[42] Jiang S, Dai LX, Chen H, Hu HP, Jiang W, Chen XD. Folding beam-type piezoelectric phononic crystal with a low-frequency and broad band gap. Appl Math Mech Eng Ed 2017;38:411–22.
[43] Coffy E, Lavergne T, Addouche M, Euphrasie S, Vairac P, Khelif A. Ultra-wide acoustic band gaps in pillar-based phononic crystal strips. J Appl Phys 2015;118:214902.